Key Points:
- Six Psw enhancement-induced ULF waves with increasing amplitudes were observed
- The wave amplitude could increase four times in several wave periods
- Superposition of two wave modes could cause the wave amplitude increase

Magnetospheric ULF waves with increasing amplitude related to solar wind dynamic pressure changes: The Time History of Events and Macroscale Interactions during Substorms (THEMIS) observations

X. C. Shen[1,2,3], Q.-G. Zong[3], Q. Q. Shi[1], A. M. Tian[1], W. J. Sun[3], Y. F. Wang[3], X. Z. Zhou[3], S. Y. Fu[3], M. D. Hartinger[4], and V. Angelopoulos[5]

[1]Shandong Provincial Key Laboratory of Optical Astronomy and Solar-Terrestrial Environment, School of Space Science and Physics, Shandong University, Weihai, China, [2]State Key Laboratory of Space Weather, Center for Space Science and Applied Research, Chinese Academy of Sciences, Beijing, China, [3]School of Earth and Space Sciences, Peking University, Beijing, China, [4]Atmospheric, Oceanic, and Space Sciences Department, University of Michigan, Ann Arbor, Michigan, USA, [5]Earth and Space Sciences Department, University of California, Los Angeles, California, USA

Abstract Ultralow frequency (ULF) waves play an important role in transferring energy by buffeting the magnetosphere with solar wind pressure impulses. The amplitudes of magnetospheric ULF waves, which are induced by solar wind dynamic pressure enhancements or shocks, are thought to damp in one half a wave cycle or an entire wave cycle. We report in situ observations of solar wind dynamic pressure impulse-induced magnetospheric ULF waves with increasing amplitudes. We found six ULF wave events induced by solar wind dynamic pressure enhancements with slow but clear wave amplitude increase. During three or four wave cycles, the amplitudes of ion velocities and electric field of these waves increased continuously by 1.3–4.4 times. Two significant events were selected to further study the characteristics of these ULF waves. We found that the wave amplitude growth is mainly contributed by the toroidal mode wave. Three possible mechanisms of causing the wave amplitude increase are discussed. First, solar wind dynamic pressure perturbations, which are observed in a duration of 20–30 min, might transfer energy to the magnetospheric ULF waves continually. Second, the wave amplitude increase in the radial electric field may be caused by superposition of two wave modes, a standing wave excited by the solar wind dynamic impulse and a propagating compressional wave directly induced by solar wind oscillations. When superposed, the two wave modes fit observations as does a calculation that superposes electric fields from two wave sources. Third, the normal of the solar wind discontinuity is at an angle to the Sun-Earth line. Thus, the discontinuity will affect the dayside magnetopause continuously for a long time.

1. Introduction

Jacobs et al. [1964] divided ultralow frequency (ULF) waves into several categories, including Pi waves for irregular oscillations lasting a few wave periods and Pc waves for quasi-sinusoidal oscillations lasting relatively longer. In recent years, the important roles of these wave in the magnetosphere has been uncovered. They are, for example, thought to modulate the dynamics of energetic particles [e.g., *Southwood and Kivelson*, 1981; *Baumjohann et al.*, 1983; *Zong et al.*, 2009], contribute to electron dropout in the outer radiation belt [e.g., *Loto'aniu et al.*, 2010; *Turner et al.*, 2012], and excite auroral activity [e.g., *Greenwald and Walker*, 1980; *Samson et al.*, 1996].

Although mechanisms that excite magnetospheric ULF waves have been studied for many years, no consensus regarding them has been reached. Early results show that the Kelvin-Helmholtz instability [*Pu and Kivelson*, 1983] on the magnetopause could transfer energy into the magnetosphere and excite field line resonance [e.g., *Hudson et al.*, 2004; *Rae et al.*, 2005; *Claudepierre et al.*, 2008]. Some works show that a solar wind dynamic pressure impulse may excite ULF waves in the magnetosphere [e.g., *Tan*, 2004; *Zong et al.*, 2009; *Zhang et al.*, 2010; *Shi et al.*, 2013]. *Kepko* [2002, 2003] proposed that quasi-monochromatic pulsations in the solar wind (rather than pulses) could directly drive magnetospheric pulsations. These waves could also be induced by internal processes, such as substorms [e.g., *Olson*, 1999; *Hsu and McPherron*, 2007; *Hao et al.*, 2014] or drift-bounce resonance with ring current ions [*Southwood et al.*, 1969].

Ultralow frequency waves in the magnetosphere are classified as toroidal mode or poloidal mode, according to the direction of magnetic field perturbations. Toroidal mode waves have a magnetic field that oscillates azimuthally; poloidal mode waves have a magnetic field that oscillates radially [*Sugiura and Wilson*, 1964].

Although most ULF waves have been observed in the dayside magnetosphere [e.g., *Kaufmann and Walker*, 1974; *Nopper et al.*, 1982; *Wilken et al.*, 1982; *Baumjohann et al.*, 1984; *Cahill et al.*, 1990; *Zong et al.*, 2007; *Sarris et al.*, 2010; *Takahashi et al.*, 2010; *Hartinger et al.*, 2011], *Tian et al.* [2012] observed a ULF wave driven by the cavity/waveguide modes in the magnetotail. *Shi et al.* [2013] reported ULF waves induced by sudden impulses (SIs) in the nightside magnetosphere, and they propose that these waves are closely related to vortices. Recently, they reported the first in situ observation of vortices induced by an increase in solar wind pressure [*Shi et al.*, 2014].

The time evolution of nightside ULF wave activity is highly variable. Which factors contribute most strongly to this variability is unknown, but wave damping is likely one of the most important. Ultralow frequency wave energy could decay via several mechanisms, two of which are considered as critical energy sinks. One is Joule dissipation in the ionosphere for standing Alfvén waves [*Greenwald and Walker*, 1980]; the other is Landau damping, which transfers wave energy to particles [*Landau*, 1946]. In addition, wave energy can leak out of the magnetosphere via the magnetopause [*Mann and Wright*, 1999] or magnetotail [*Samson et al.*, 1992]. Thus, after generation almost all reported ULF waves have decreasing wave amplitudes [e.g., *Zong et al.*, 2009; *Shi et al.*, 2013; *Samsonov et al.*, 2014]. Previous three-dimensional simulations of magnetosphere MHD waves driven by sudden impulses [*Lee and Hudson*, 2001; *Chi et al.*, 2006] show that single field-line resonance could result in slow rise at off-equator regions.

In this article, however, we will study waves with increasing amplitudes near the equatorial plane by using in situ observations to better understand the factors affecting the time evolution of nightside ULF wave activity. In section 2, we will briefly illustrate the data sources. Section 3 shows the observations and analysis of two events. The last section will be discussion and summary.

2. Data Set

In this study, we use data from the Time History of Events and Macroscale Interactions during Substorms (THEMIS) mission [*Angelopoulos*, 2008], which consists of five identical probes (THA, THB, THC, THD, and THE). Each probe is equipped with a fluxgate magnetometer [*Auster et al.*, 2008], which provides magnetic field data; an electrostatic analyzer (ESA) [*McFadden et al.*, 2008], which provides thermal (5 eV to 25 keV) ion and electron data; and an electric field instrument (EFI) [*Bonnell et al.*, 2008], which provides 2-D electric field in the spin plane. We use 3 s resolution spin-fit data from those instruments. Data from THEMIS ground-based observatories are also used [*Mende et al.*, 2009]. Interplanetary magnetic field (IMF) and plasma data, which are time shifted to the Earth's bow shock nose, are from OMNI [*King and Papitashvili*, 2005].

3. Observations

Using IMF and solar wind plasma data obtained from OMNI, we reviewed solar wind dynamic pressure enhancement events from March 2007 to December 2012. The solar wind dynamic pressure enhancement is defined as a 0.5 times step-like rise in fewer than 10 s and stable pressure for at least 10 min upstream and downstream of the pressure increase front. Magnetospheric responses to these enhancements were evaluated one by one. Sixty-four ULF wave events were observed by THEMIS satellites. Of these events, six display gradual increases in amplitudes of ion velocity and electric field perturbations. The variable γ, defined as the ratio of the amplitudes (absolute value) of each half period to the first half period $\left(\left|\frac{A_i}{A_1}\right|\right)$, is used to check ULF wave amplitude growth. We calculated the γ values from ion velocity and electric field data. Figure 1 shows the γ of (a) ion velocity and (b) electric field for the six events listed in Table 1 ($\gamma_{Vi-\max}$ represents the maximum γ of the ion velocity).

3.1. THEMIS Observation

To further study ULF wave characteristics, we choose two events (the 1 April 2011 and 6 September 2012). Figure 2 shows the locations of THA and THB during those events. During both, THB was in the solar wind and THA was on the dawn and dusk sides of the inner magnetosphere. Because THD and THE were very close to THA during both events, they observed nearly identical plasma and magnetic field variations. Similar IMF and
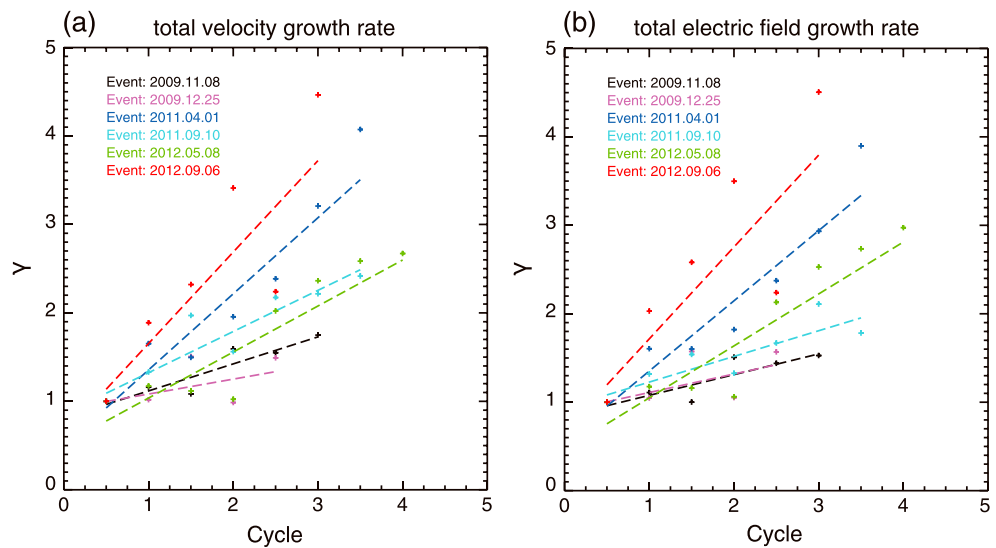
Figure 1. Wave amplitude increase versus wave cycle of (a) ion velocity and (b) electric field for six magnetospheric ULF wave events. Electric fields are calculated by $V_i \times B$. γ is defined as the amplitude of each half wave period divided by the amplitude of the first half wave period. Crosses represent calculated γ.

plasma data were obtained by THB and THC, which were in the solar wind. Thus, we choose THB to monitor the solar wind variation and THA to show the magnetospheric response.

Figure 3 is an overview of the 1 April 2011 (Event A) and 6 September 2012 (Event B) events. All quantities in Figure 3 are in GSM coordinates. Figures 3a and 3b show the IMF and the solar wind dynamic pressure from THB. The observations of THB were time shifted by 827 s for Event A and −320 s for Event B according to the propagation speeds of the shocks and the separations between THB and THA. The shocks were identified by sharp (> 1.2 nPa within 5 s) dynamic pressure increases and also by directional change in the magnetic field, which is marked by the red vertical dashed lines. The magnetic latitude, local time, and L shell information of THA are labeled on the bottom of Figure 3. For both events, the variations of L values of THA were lower than 0.5 R_E during the time interval concern. Therefore, the frequency variation of the field lines observed by the THA should also be limited. In addition, the magnetic latitudes of THA were lower than 10° from the equator, which indicates that the satellites may be located near the wave node of the field line fundamental oscillation. THEMIS-A was located in the northern hemisphere for both events.

Figure 3 also shows THA observations of (c) magnetic field components, (d) ion density, (e) total ion velocity, (f) ion velocity components, and (g) ion temperature components. Figures 3f1 and 3f2 show that a clear ULF wave was excited with the arrival of interplanetary dynamic pressure enhancements for both events. More interestingly, the amplitudes of ion velocities continued increasing during three or four wave cycles. Note that the period of density fluctuation matches that of V_x for Event A, whereas the period of density fluctuation does not match that of V_x for Event B. From wavelet analysis (not shown), two typical frequencies, $\sim$2 mHz and $\sim$ 4 mHz, were captured. The $\sim$ 4 mHz density fluctuation in this event may be caused by acceleration of cold particles [*Sakurai et al.*, 1999], which is consistent with the fluctuation in total velocity shown in Figure 3e2. In addition, the density fluctuation has a wave frequency of around $\sim$2 mHz, which is associated with compressional waves.

Table 1. THEMIS Observations of Wave Amplitude Increases

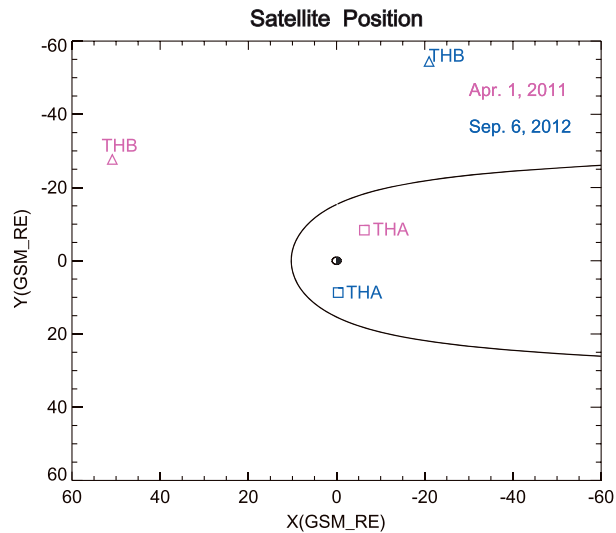| No.	Date (yyyy/mm/dd)	Locations (GSM: x, y, z)	MLAT (deg)	$\gamma_{Vi-\mathrm{max}}$	Increasing Periods
1	2009/11/08	(3.0, −6.9, −0.8)	−5.9	1.6	3
2	2009/12/25	(−1.8, −8.9, −1.2)	−7.7	1.3	3
3	2011/04/01	(−6.3, −8.4, 1.6)	8.8	4.0	3
4	2011/09/10	(−0.4, 10.3, 0.0)	0.1	2.1	4
5	2012/05/08	(−3.8, −8.3, 0.5)	3.2	2.6	4
6	2012/09/06	(−0.5, 8.9, 0.5)	3.5	4.4	4

Figure 2. The locations of THA and THB for two events. The purple symbols are for the 1 April 2011 event (Event A), and the blue symbols are for the 6 September 2012 event (Event B). The curved black line indicates the location of the magnetopause, which is calculated from the *Shue et al.* [1998] model using the solar wind dynamic pressure $D_p = 2.0$ nPa and $B_z = 1.0$ nT.

Figure 4 shows the solar wind dynamic pressure (*Psw*) and the wavelet analysis of *Psw* for both events. In addition to the sharp increases in *Psw*, significant wave signatures, with a frequency of ~2 mHz, were observed.

We performed a wavelet transform on the electric field (calculated by $V_i \times B$) to find the precise ULF wave frequency (shown in Figure 5). For Event A, the frequency of wave power in all three components ranges from 1.9 to 2.7 mHz (shown in Figures 5b1–5d1), which is in the Pc5 range. For Event B, the typical frequency is
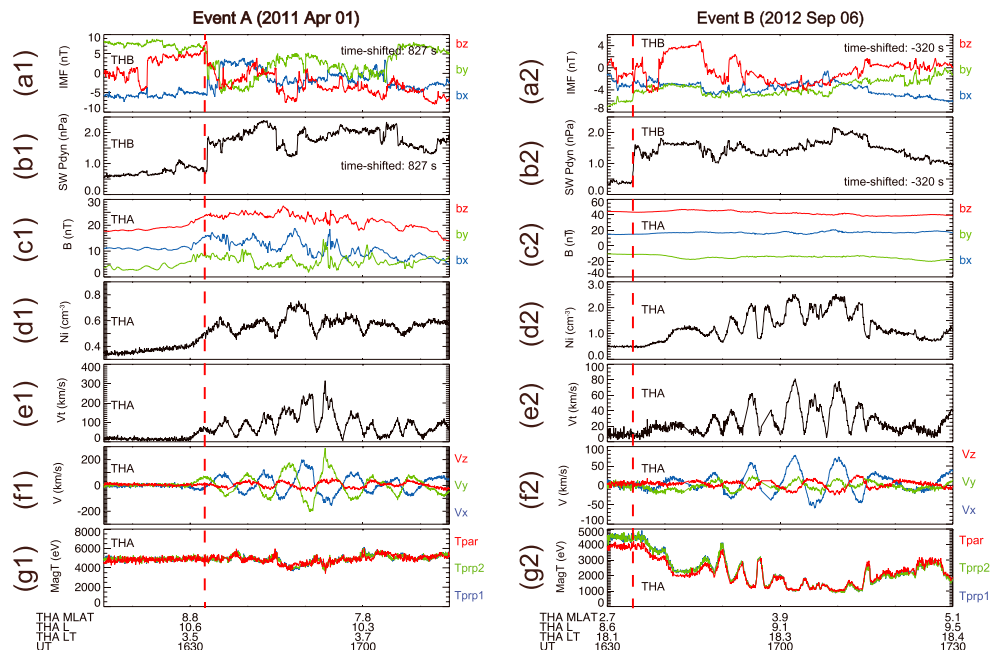

Figure 3. Overview of two events from 16:15 to 17:15 UT on 1 April 2011 (Event A) and 16:30 to 17:30 UT on 6 September 2012 (Event B). (a) IMF, (b) solar wind dynamic pressure, (c) magnetospheric magnetic field components, (d) ion density, (e) total ion velocity, (f) ion velocity, and (g) ion temperature. The solar wind and IMF data are time shifted as labeled in the panels. The red vertical dashed lines indicate the sudden enhancements of the solar wind dynamic pressure.
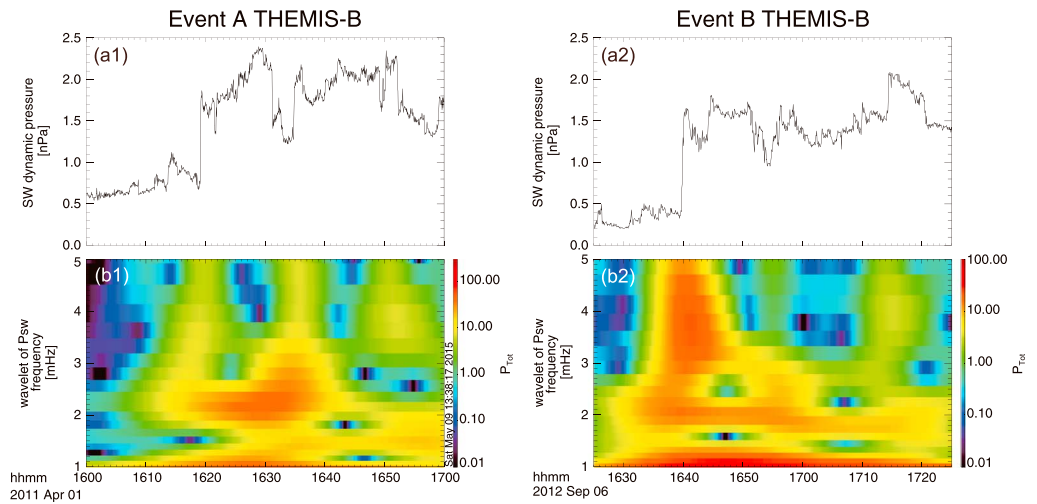
Figure 4. The (a) solar wind dynamic pressure fluctuations and (b) their wavelet analyses for Events A and B.

clear from 1.8 to 2.5 mHz (shown in Figures 5b2–5d2), also in the Pc5 range. The typical frequency bands of the two events are marked in the last three panels. For both events, after the waves were induced, the wave power between the typical frequency bands enhanced rapidly and remained high for more than half an hour.

In Figure 6, we adopted the field-aligned coordinate (FAC) system [e.g., *Takahashi et al.*, 1990; *Hartinger et al.*, 2011]. In that system, *r* points approximately radially outward; *a* points azimuthally eastward; and *p* is along the background magnetic field direction, which is obtained from the 15 min sliding averaged magnetic field.
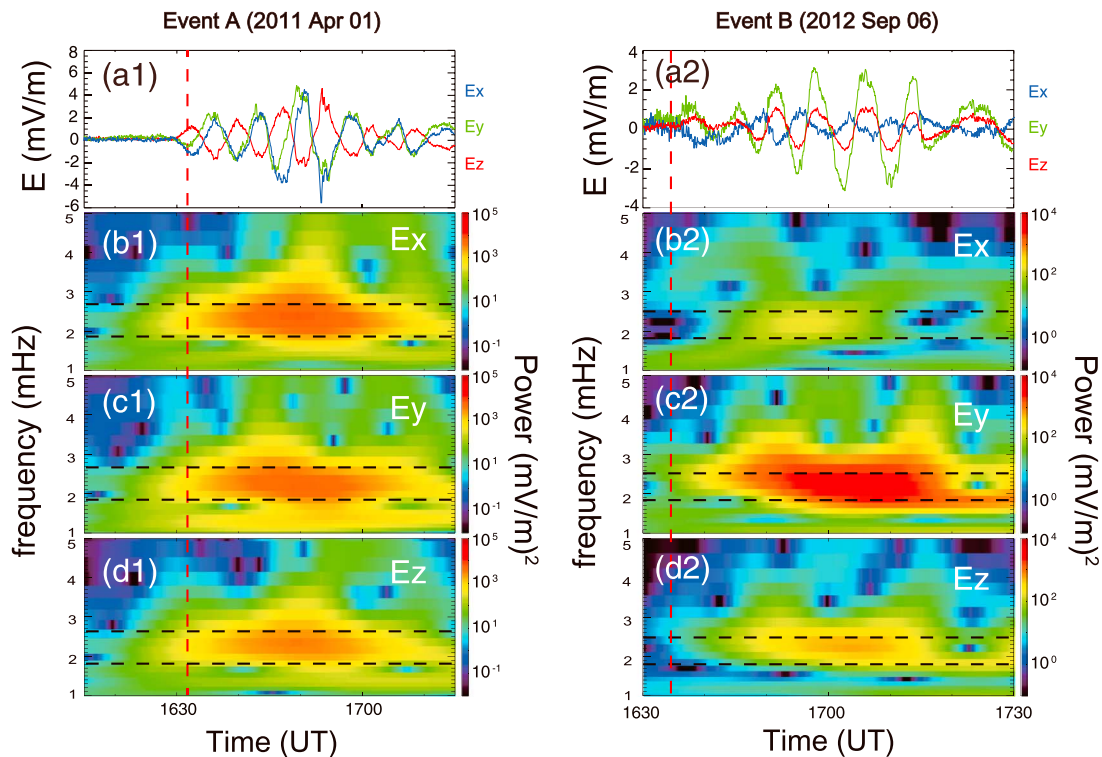

Figure 5. Wavelet analysis of the electric field (obtained from $V_i \times B$) for Event A (1 April 2011) and Event B (6 September 2012). (a) Three components of the electric field in GSM coordinates and the wavelet analysis of the (b) *x*, (c) *y*, and (d) *z* components of the electric field. The dashed lines in the last three panels mark the strongest frequency bands. For Event A, the frequency of wave power in all three components ranges from 1.9 to 2.7 mHz. For Event B, the typical frequency is clear from 1.8 to 2.5 mHz. The red vertical dashed lines indicate the sudden enhancements in the solar wind dynamic pressure.
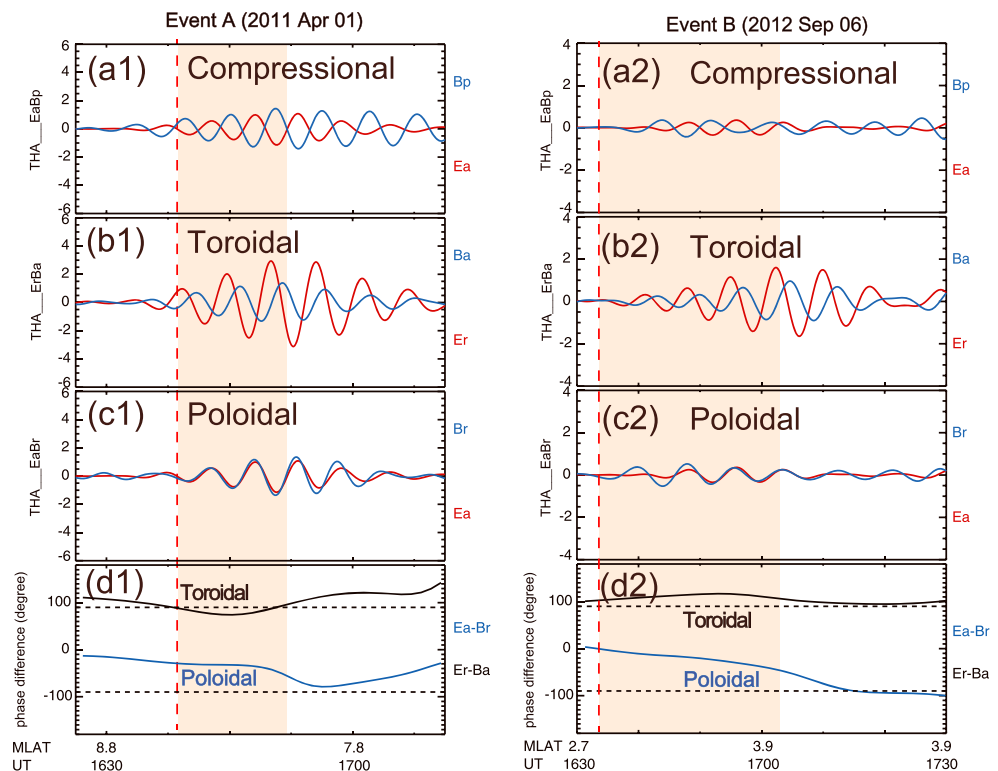
Figure 6. Magnetic and electric fields in field-aligned coordinates (FACs) and phase differences between their components for Events A and B. (a) B_p-E_a, (b) B_a-E_r, (c) B_r-E_a, and (d) phase difference between the magnetic and electric fields. The data have been band-pass filtered in the range of 1.9 to 2.7 mHz for Event A and 1.8 to 2.5 mHz for Event B. The black dashed lines in Figure 6d mark the $\pm 90°$. Note that in both events, the waves are standing in toroidal mode but propagating in poloidal mode. The red vertical dashed lines indicate the sudden enhancements in the solar wind dynamic pressure.

The band-pass-filtered magnetic field (blue lines in Figures 6a–6c) and electric field (red lines in Figures 6a–6c) were projected onto the FAC system. The frequency bands used in this wave mode analysis are the same bands indicated by the horizontal dashed lines in Figure 5 (those corresponding to power enhancements).

Figure 6a shows perturbations in E_a and the compressional component B_p, which are typically associated with fast mode waves. Perturbations in E_r and B_a, which are associated with toroidal modes, are presented in Figure 6b. Figure 6c shows perturbations in E_a and B_r, which are associated with poloidal modes. In Event A, both the amplitudes of poloidal mode and toroidal mode waves are growing. In Event B, the amplitude of toroidal mode wave is increasing, whereas that of the poloidal mode wave is decreasing. Moreover, the amplitude of the poloidal mode wave is much smaller than that of the toroidal mode wave in Event B. Figure 6d illustrates the E-B phase differences of toroidal mode (black lines) and poloidal mode (blue lines) waves. The phase differences are calculated for the waves with typical frequencies, 2.3 mHz for Event A and 2.2 mHz for Event B. After a dynamic pressure impulse arrived at the magnetosphere, the phase differences for toroidal mode waves (black lines) were around 90°, which is consistent with a standing wave signature, whereas the poloidal mode waves (blue lines) were not standing in both events.

3.2. Ground-Based Observation

Figure 7 shows the magnetic field H components from geomagnetic stations located near the magnetic latitude (MLAT) of the satellite footprints for both events. For Event A, magnetic field H components are obtained from the KAKO, INUV, SNAP, RANK, and KUUJ ground stations (their locations are labeled on each figure panel). Clear ULF wave signatures were captured by these stations. The main frequency is consistent with that from the THEMIS observations. The data are band-pass filtered from 1.9 mHz to 2.7 mHz, which shows that magnetic field H component wave amplitude increases 2.4 to 4.1 times after wave induction. The clear wave amplitude increase was observed in large longitudinal regions from geomagnetic longitude 264.9° to 13.4° (the longitudinal separation is 108.5° or 7.2 magnetic local time (MLT)). A similar phenomenon also appeared in the
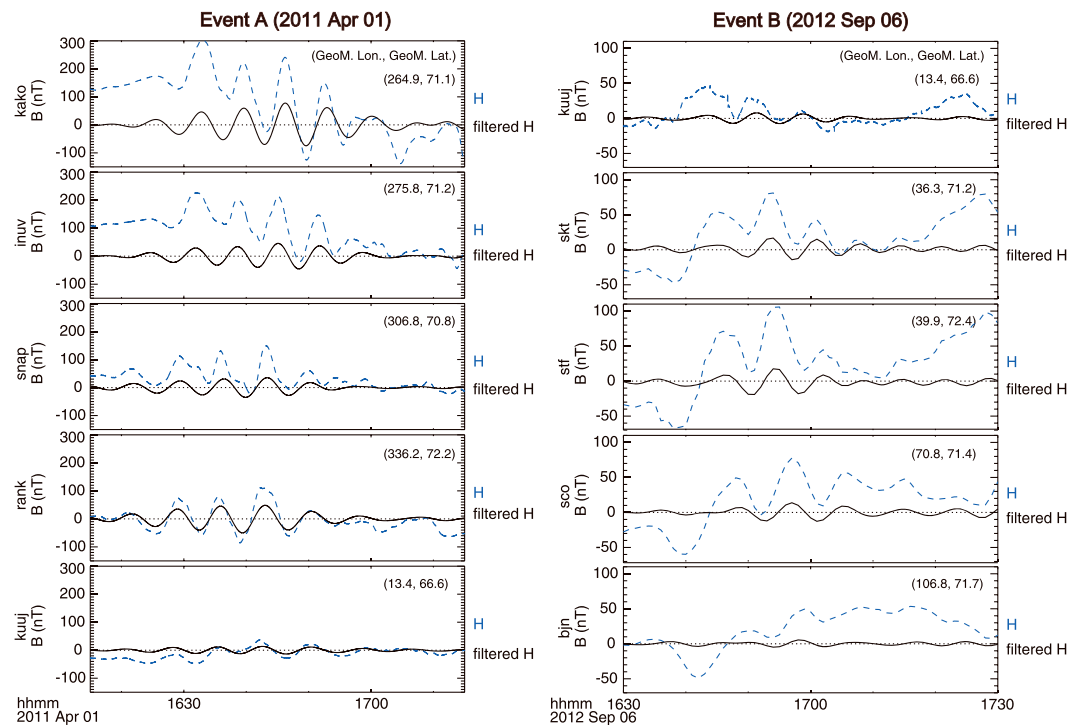
Figure 7. Magnetic field *H* components from geomagnetic (GMAG) stations for (left) Event A and (right) Event B. Blue dashed line indicates the magnetic field *H* component, and black solid line indicates the filtered magnetic field *H* component. For Event A, the data are filtered from 1.9 mHz to 2.7 mHz; for Event B, the data are filtered from 1.8 to 2.5 mHz.

B event, in which the amplitudes of the relevant waves grew (1.8 to 4.4 times). The wave activity spans a longitudinal separation of about 6.2 MLT. The geomagnetic field data indicate that the observed ULF wave events presented here occurred globally.

Ground-based magnetic field data were further used to calculate the wave number for Event A. We know the wave number $m = \delta\phi/\delta\lambda$ [*Sarris et al.*, 2009], where $\delta\phi$ represents the phase difference of the *H* magnetic field component and $\delta\lambda$ is the azimuthal separation (i.e., longitudinal difference) between the two stations. When calculating the wave number, even a small separation in geomagnetic latitude between two stations may result in considerable error [*Sarris et al.*, 2013]. To minimize error, we choose stations with small differences in geomagnetic latitudes (fewer than 0.5°; see Table 2). The geomagnetic longitude and latitude of the footprint of THA at 16:00 UT were 188.9° and 71.3°, respectively. First, we choose two close stations, KAKO and INUV, with azimuthal separation $\delta\lambda = 10.92$. Figures 8a1–8d1 show ground-based observations of waves from a pair of ground stations located near the footprint of THA in Event A. Figures 8a1 and 8b1 show the wavelet power spectra of magnetic field *H* components of two stations, and the *H* components of magnetic fields are overplotted. Both stations captured significant wave signatures. The typical frequency is around 2.5 mHz for both stations. The squared wavelet coherence between magnetic field *H* components of two stations is shown in Figure 8c1. The black solid lines in Figures 8a–8c mark the main frequency 2.5 mHz used to calculate the phase difference, as shown in Figure 8d1. The green, black, and red lines show the phase differences between waves in 2.4, 2.5, and 2.7 mHz in Figure 8d1. The phase differences tend to be stable between 16:28 (UT) and 16:50 (UT). We obtain the phase difference as $\sim(360n + 45)°$ around 16:30 (UT). Using the same method, one more phase difference is calculated as $\sim(360n' + 170)°$ from another pair of stations, KAKO and SNAP, with

Table 2. Wave Numbers Calculated From the Ground Station Observations

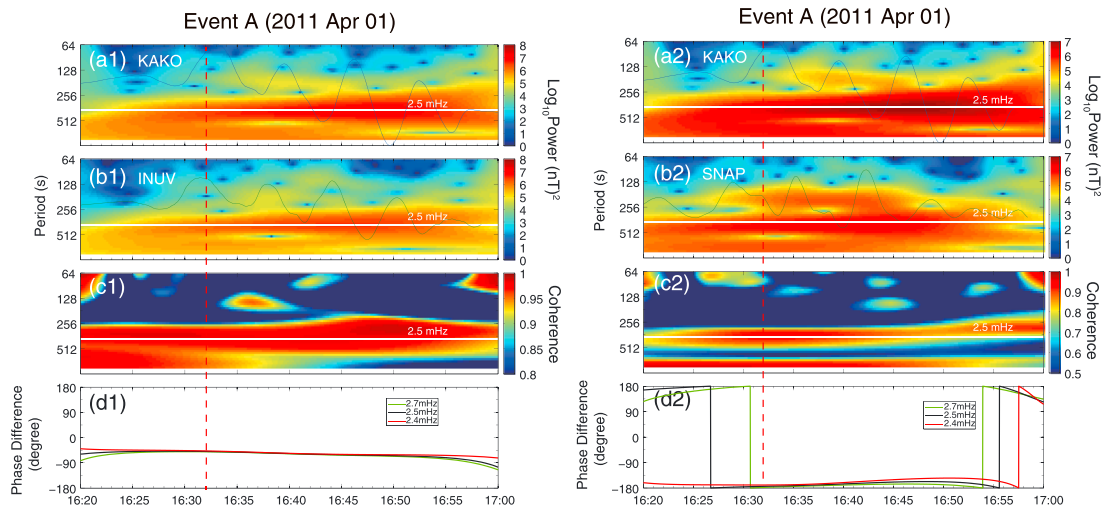| Date (yyyy/mm/dd)	Station 1 (GeoM: Lat., Long.)	Station 2 (GeoM: Lat., Long.)	$\delta\phi$ (deg)	$\delta\lambda$ (deg)	m
2011/04/01	KAKO (71.1, 264.8)	INUV (71.2, 275.8)	≈45	10.92	≈4.12
2011/04/01	KAKO (71.1, 264.8)	SNAP (70.8, 306.8)	≈170	41.93	≈4.05

Figure 8. Magnetic field H components from GMAG stations and their phase differences for Event A. (a and b) The wavelet analysis of the magnetic field H component. Magnetic field H component data are overplotted on each panel. (c) The squared wavelet coherence between magnetic field H components from two stations. The white solid lines in Figures 8a–8c mark the frequency of 2.5 mHz, which is used to calculate (d) the phase difference between two H components. The red vertical dashed lines indicate the sudden enhancements in the solar wind dynamic pressure.

larger separation in the azimuthal direction ($\delta\lambda = 41.93$; see Figures 8a2–8d2). The ratio of these two phase differences and the ratio of two longitudinal differences of two pairs of stations should be equal. Thus, n and n' are calculated as 0. Given that the magnetic longitude difference between the two stations is 10.92° (shown in Table 2), for the first pair of stations the wave number is calculated as ≈ 4.12. Similarly, for the second pair of stations, the wave number is ≈ 4.05 (shown in Table 2). The small wave number indicates that the standing toroidal wave may be driven by a waveguide mode [e.g., *Hudson et al.*, 2004]. For Event B, the stations located near the footprint of THA (GeoM: long. 12.0°, lat. 72.2°) did not provide high time resolution magnetic field data. Thus, the wavenumber for Event B was not calculated.

4. Discussion

The amplitudes of magnetospheric ULF waves, which are induced by solar wind dynamic pressure enhancements or shocks, are thought to damp rapidly. However, in the six Pc5 wave events we observed, the wave amplitudes of ion velocities and electric fields could increase gradually by more than four times during three or four cycles.

4.1. Solar Wind Discontinuity Normal Direction

An amplitude increase may occur because the normal of the solar wind discontinuity is at an angle to the Sun-Earth line. Thus, the discontinuity will affect the dayside magnetopause continuously for a long time. Interaction between the discontinuity and the magnetosphere at various locations and at various times may cause compressional waves to be launched, and superposition of these waves may result in a slow increase in toroidal wave amplitude. We calculated the normal directions of solar wind discontinuities for the two events using the Timing method [*Russell et al.*, 1983]. They are [$-0.90, -0.41, -0.10$] (calculated from Cluster's four satellites) and [$-0.94, 0.13, 0.31$] (calculated from THEMIS-B, THEMIS-C, Wind, and ACE satellites). The angle between the normal direction of the solar wind discontinuity and the Sun-Earth line is about 26° for Event A and 20° for Event B. The velocities of the discontinuities, obtained from the Timing method, are 330 km/s for Event A and 484 km/s for Event B. However, these angles are not large enough to produce a gradual increase in wave amplitude for nearly half an hour in the two events.

4.2. Solar Wind Dynamic Pressure Perturbations

Wave signatures with frequencies around 2 mHz were captured in solar wind dynamic pressures for both events (see Figure 4). The wave power in Figure 4b shows that both Psw oscillations in the two events lasted for almost half an hour. Compressional waves, which could be induced by the Psw oscillations [*Kepko*, 2002, 2003], continuously couple to the standing toroidal mode wave for about half an hour. Furthermore, the time scales of wave amplitude increases shown in Figure 3 are between 20 and 30 min. Thus, we suggest that one wave energy input could be Psw perturbation.
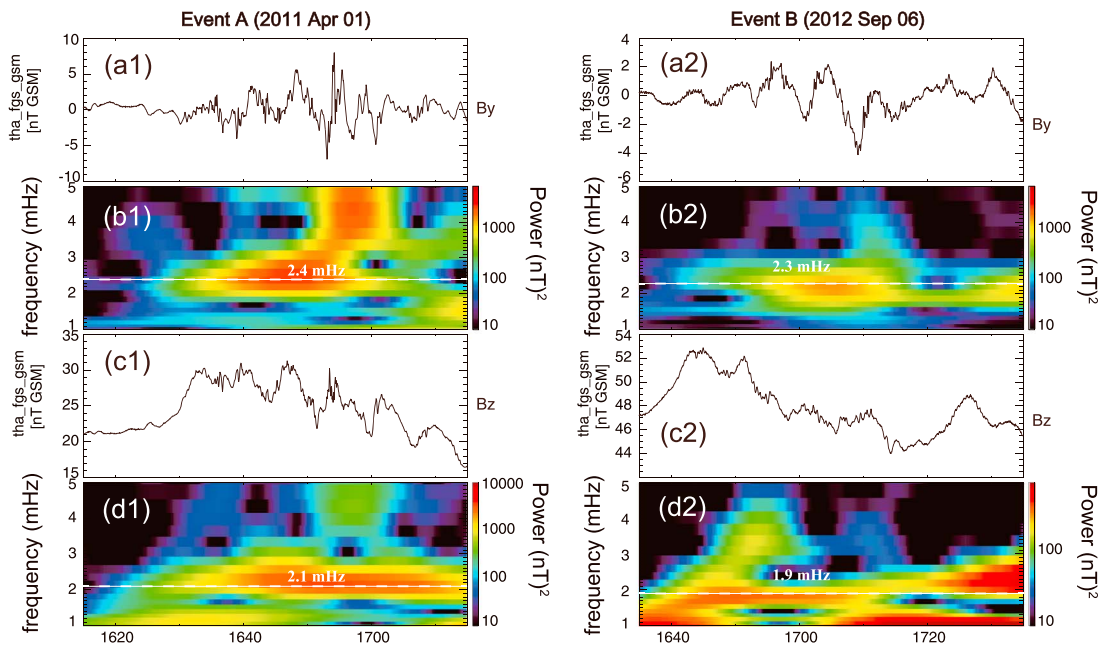
Figure 9. The parallel and azimuthal magnetic field components and their wavelet analyses for Events A and B. (a) B_a, (b) wavelet analysis of B_a, (c) B_p, and (d) wavelet analysis of B_p. The typical frequencies for B_a and B_p are marked by dashed white lines, and the values are labeled above the lines.

4.3. Wave Mode Superposition

The wave energy peaks in *Psw* are 2.1 mHz and 2.0 mHz at 16:24 UT and 16:44 UT (without time shift) for the two events, respectively (see Figure 4), and the frequencies of the toroidal mode waves are 2.4 mHz and 2.3 mHz (shown in Figure 9b). Even though the frequencies of *Psw* oscillations are extremely close to that of the magnetic field azimuthal component observed in the magnetosphere, a small difference between them still exists. Therefore, another scenario, superposition of two wave modes, is discussed. One wave mode is a standing wave excited by a sharp solar wind dynamic impulse, as shown in Figure 3b. The magnetic field lines are continuously shaken by traveling compressional waves, as indicated by continuous oscillations in the magnetic field p component (i.e., along the magnetic field line) (shown in Figure 9c). *Kepko* [2002, 2003] proposed that the pressure balance between the inside and the outside of the magnetosphere could cause magnetospheric ULF waves to be directly excited by solar wind dynamic pressure perturbations. Significant wave power around ∼ 2 mHz was observed in the solar wind dynamic pressure for the two events (see Figure 4). Thus, the traveling compressional wave in both events might be directly driven by solar wind dynamic pressure perturbations, and the compressional wave frequency might be controlled by the frequency of the solar wind dynamic pressure perturbations [*Kepko*, 2003]. The electric field of the standing wave oscillates radially, and the electric field of the compressional wave oscillates radially and azimuthally. Thus, electric fields of two wave sources may superpose in the radial direction. We calculate the superposition of two waves for two events. The functions of the two wave sources are as follows:

$$\psi_1 = A_1 \cos(\varphi_1 - \omega_1 t) \tag{1}$$

$$\psi_2 = A_2 \cos(\varphi_2 - \omega_2 t) \tag{2}$$

After superposing these two waves, the wave function changes to

$$\psi_{superposed} = \psi_1 + \psi_2 = A_1 \cos(\varphi_1 - \omega_1 t) + A_2 \cos(\varphi_2 - \omega_2 t) \tag{3}$$

If two wave sources with very close frequencies and amplitudes are superposed on a wave, the amplitude of that wave will vary from a minimum to a maximum value. This type of wave is called a beat wave. We used the same amplitude for two waves in the calculation (i.e., $A_1 = A_2 = A_0$). The decay effect has also been considered. The filtered E_r component in Figure 6 shows that wave signatures are observed during 1 h. We consider the wave amplitude decrease to $1/e$ times the initial amplitude in 1 h. Thus, the decay factor is $e^{-\frac{t}{3600}}$.
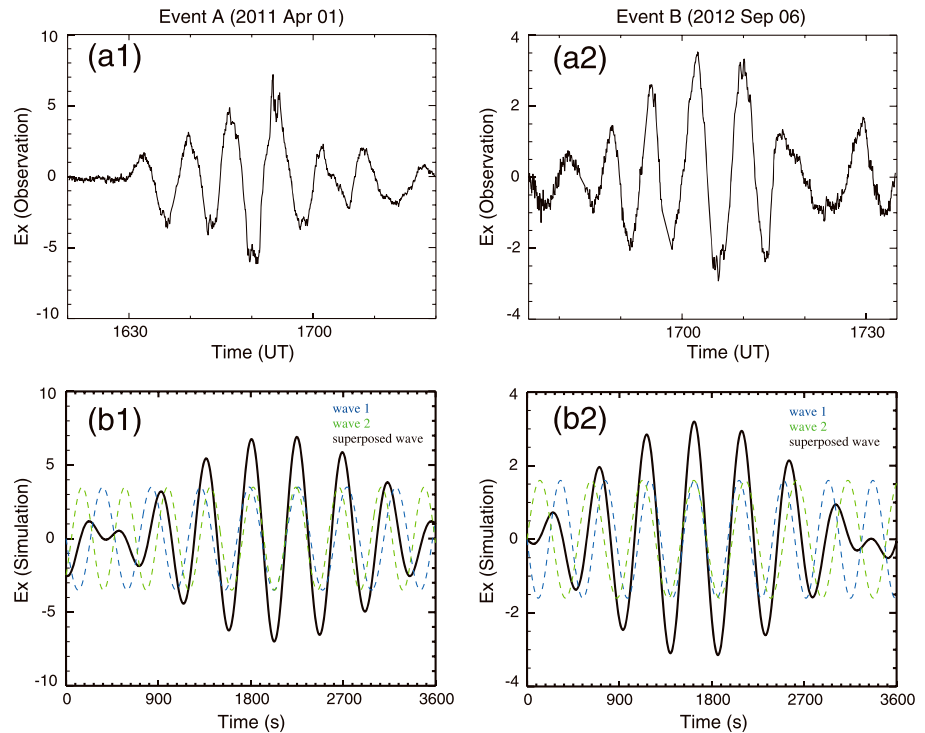
Figure 10. The observed and simulated E_r for Events A and B. (a) The *radial* component of the unfiltered electric field in the FAC system from 16:20 to 17:20 UT observed by THA and (b) the *radial* component of the electric field calculated by superposition of two wave sources. In Figure 10b, the blue and green dashed lines indicate two wave sources and the black solid lines illustrate the superposed waves.

Therefore, the superposed wave in our calculation was modified as follows:

$$\psi_{\text{superposed}} = \psi_1 + \psi_2 = 2A_0 e^{-\frac{t}{3600}} \cos\left(\frac{(\varphi_1 + \varphi_2) - (\omega_1 + \omega_2)t}{2}\right) \cos\left(\frac{(\varphi_1 - \varphi_2) - (\omega_1 - \omega_2)t}{2}\right) \quad (4)$$

In the calculation, the frequencies for two wave sources are determined by wavelet analyses of B_a and B_p (shown in Figure 9), because B_a is associated with a toroidal mode wave and B_p is associated with a compressional wave. For Event A, $\omega_1 = 2.4$ mHz and $\omega_2 = 2.1$ mHz; for Event B, $\omega_1 = 2.3$ mHz and $\omega_2 = 1.9$ mHz. The phases of the waves are defined to match the observed beat wave. For Event A, $A_0 = 3.5$, $\varphi_1 = -\frac{1}{2}\pi$, $\varphi_2 = -\frac{5}{4}\pi$; for Event B, $A_0 = 1.7$, $\varphi_1 = -\frac{1}{2}\pi$, $\varphi_2 = -\frac{3}{2}\pi$.

Figure 10b shows the superposition of these two wave sources. In these two events, the time scale of wave amplitude increase and decrease in the calculation matches the observations fairly well. Almost half an hour and three periods were required to reach maximum wave amplitude. The waves damp within the next half an hour and three periods. Therefore, the wave amplitude increase could be caused by superposition of two wave sources.

5. Summary

Previous observations show that after induction most magnetospheric ULF waves decrease in wave amplitude. By checking the responses of the magnetosphere to dynamic pressure enhancements from 1 April 2007 to 31 December 2012, we found six ULF waves with slow but clear wave amplitude increase.

Two significant events were chosen to further study the characteristics of these ULF waves. Both events show that the wave amplitude increases were mostly contributed by toroidal mode standing waves. Three wave amplitude increase mechanisms are discussed. First, because the normal of the solar wind discontinuity is at an angle to the Sun-Earth line, the discontinuity will affect the dayside magnetopause continuously for a long time. Second, solar wind dynamic pressure perturbations, observed for 20–30 min, could continuously

transfer energy to magnetospheric ULF waves. Third, two wave modes, a standing wave excited by the solar wind dynamic impulse and a propagating compressional wave directly induced by solar wind oscillations, could superimpose, causing a wave amplitude increase in the radial electric field.

Our main conclusions are summarized below:

1. We found six ULF waves with slow but clear wave amplitude increase. The amplitudes of ion velocities and electric field of these waves increased continuously by a factor of 1.3–4.4 during three to four wave cycles.
2. According to our case studies of Events A and B, the wave amplitude increases were mostly contributed by toroidal mode standing waves.
3. Three factors, (1) normal direction of solar wind discontinuities, (2) solar wind dynamic pressure perturbations, and (3) wave mode superposition, could contribute to these increases.
4. Wave mode superposition could be responsible for the wave amplitude increases in Events A and B.

References

Angelopoulos, V. (2008), The THEMIS mission, *Space Sci. Rev.*, *141*, 5–34, doi:10.1007/s11214-008-9336-1.

Auster, H. U., et al. (2008), The THEMIS fluxgate magnetometer, *Space Sci. Rev.*, *141*, 235–264, doi:10.1007/s11214-008-9365-9.

Baumjohann, W., O. H. Bauer, G. Haerendel, H. Junginger, and E. Amata (1983), Magnetospheric plasma drifts during a sudden impulse, *J. Geophys. Res.*, *88*, 9287–9289, doi:10.1029/JA088iA11p09287.

Baumjohann, W., H. Junginger, G. Haerendel, and O. H. Bauer (1984), Resonant Alfvén waves excited by a sudden impulse, *J. Geophys. Res.*, *89*(A5), 2765–2769, doi:10.1029/JA089iA05p02765.

Bonnell, J., F. Mozer, G. Delory, A. Hull, R. Ergun, C. Cully, V. Angelopoulos, and P. Harvey (2008), The electric field instrument (EFI) for THEMIS, *Space Sci. Rev.*, *141*(1-4), 303–341.

Cahill, L. J., N. G. Lin, J. H. Waite, M. J. Engebretson, and M. Sugiura (1990), Toroidal standing waves excited by a storm sudden commencement: DE 1 observations, *J. Geophys. Res.*, *95*, 7857–7867, doi:10.1029/JA095iA06p07857.

Chi, P. J., D.-H. Lee, and C. T. Russell (2006), Tamao travel time of sudden impulses and its relationship to ionospheric convection vortices, *J. Geophys. Res.*, *111*, A08205, doi:10.1029/2005JA011578.

Claudepierre, S. G., S. R. Elkington, and M. Wiltberger (2008), Solar wind driving of magnetospheric ULF waves: Pulsations driven by velocity shear at the magnetopause, *J. Geophys. Res.*, *113*, A05218, doi:10.1029/2007JA012890.

Greenwald, R. A., and A. D. M. Walker (1980), Energetics of long period resonant hydromagnetic waves, *Geophys. Res. Lett.*, *7*, 745–748, doi:10.1029/GL007i010p00745.

Hao, Y. X., et al. (2014), Interactions of energetic electrons with ULF waves triggered by interplanetary shock: Van Allen probes observations in the magnetotail, *J. Geophys. Res. Space Physics*, *119*, 8262–8273, doi:10.1002/2014JA020023.

Hartinger, M., V. Angelopoulos, M. B. Moldwin, K. Glassmeier, and Y. Nishimura (2011), Global energy transfer during a magnetospheric field line resonance, *Geophys. Res. Lett.*, *38*, L12101, doi:10.1029/2011GL047846.

Hsu, T., and R. L. McPherron (2007), A statistical study of the relation of Pi 2 and plasma flows in the tail, *J. Geophys. Res.*, *112*, A05209, doi:10.1029/2006JA011782.

Hudson, M. K., R. E. Denton, M. R. Lessard, E. G. Miftakhova, and R. R. Anderson (2004), A study of Pc-5 ULF oscillations, *Ann. Geophys.*, *22*, 289–302, doi:10.5194/angeo-22-289-2004.

Jacobs, J. A., Y. Kato, S. Matsushita, and V. A. Troitskaya (1964), Classification of geomagnetic micropulsations, *Geophys. J. R. Astron. Soc.*, *8*, 341–342, doi:10.1111/j.1365-246X.1964.tb06301.x.

Kaufmann, R. L., and D. N. Walker (1974), Hydromagnetic waves excited during an SSC, *J. Geophys. Res.*, *79*, 5187–5195, doi:10.1029/JA079i034p05187.

Kepko, L. (2002), ULF waves in the solar wind as direct drivers of magnetospheric pulsations, *Geophys. Res. Lett.*, *29*, 1197, doi:10.1029/2001GL014405.

Kepko, L. (2003), Observations of discrete, global magnetospheric oscillations directly driven by solar wind density variations, *J. Geophys. Res.*, *108*, 1257, doi:10.1029/2002JA009676.

King, J., and N. Papitashvili (2005), Solar wind spatial scales in and comparisons of hourly wind and ace plasma and magnetic field data, *J. Geophys. Res.*, *110*, A02104, doi:10.1029/2004JA010649.

Landau, L. (1946), On the vibrations of the electronic plasma, *J. Phys.*, *10*, 25–34.

Lee, D.-H., and M. K. Hudson (2001), Numerical studies on the propagation of sudden impulses in the dipole magnetosphere, *J. Geophys. Res.*, *106*, 8435–8446, doi:10.1029/2000JA000271.

Loto'aniu, T. M., H. J. Singer, C. L. Waters, V. Angelopoulos, I. R. Mann, S. R. Elkington, and J. W. Bonnell (2010), Relativistic electron loss due to ultralow frequency waves and enhanced outward radial diffusion, *J. Geophys. Res.*, *115*, A12245, doi:10.1029/2010JA015755.

Mann, I. R., and A. N. Wright (1999), Diagnosing the excitation mechanisms of Pc5 magnetospheric flank waveguide modes and FLRs, *Geophys. Res. Lett.*, *26*, 2609–2612, doi:10.1029/1999GL900573.

McFadden, J. P., C. W. Carlson, D. Larson, M. Ludlam, R. Abiad, B. Elliott, P. Turin, M. Marckwordt, and V. Angelopoulos (2008), The THEMIS ESA plasma instrument and in-flight calibration, *Space Sci. Rev.*, *141*, 277–302, doi:10.1007/s11214-008-9440-2.

Mende, S. B., S. E. Harris, H. U. Frey, V. Angelopoulos, C. T. Russell, E. Donovan, B. Jackel, M. Greffen, and L. M. Peticolas (2009), The THEMIS array of ground-based observatories for the study of auroral substorms, *Space Sci. Rev.*, *141*, 357–387, doi:10.1007/s11214-008-9380-x.

Nopper, R. W., W. J. Hughes, C. G. Maclennan, and R. L. McPherron (1982), Impulse-excited pulsations during the July 29, 1977, event, *J. Geophys. Res.*, *87*, 5911–5916, doi:10.1029/JA087iA08p05911.

Olson, J. V. (1999), Pi2 pulsations and substorm onsets: A review, *J. Geophys. Res.*, *104*, 17,499–17,520, doi:10.1029/1999JA900086.

Pu, Z., and M. G. Kivelson (1983), Kelvin:Helmholtz instability at the magnetopause: Solution for compressible plasmas, *J. Geophys. Res.*, *88*, 841–852, doi:10.1029/JA088iA02p00841.

Rae, I. J., et al. (2005), Evolution and characteristics of global Pc5 ULF waves during a high solar wind speed interval, *J. Geophys. Res.*, *110*, A12211, doi:10.1029/2005JA011007.

Russell, C. T., J. T. Gosling, R. D. Zwickl, and E. J. Smith (1983), Multiple spacecraft observations of interplanetary shocks: ISEE three-dimensional plasma measurements, *J. Geophys. Res.*, *88*, 9941–9947, doi:10.1029/JA088iA12p09941.

Sakurai, T., Y. Tonegawa, T. Kitagawa, M. Nowada, A. Yamawaki, T. Mukai, S. Kokubun, T. Yamamoto, and K. Tsuruda (1999), Double-frequency oscillations of low energy plasma associated with transverse Pc5 pulsations: Geotail satellite observations, *Earth Planets Space*, *51*, 43–53.

Samson, J. C., D. D. Wallis, T. J. Hughes, F. Creutzberg, J. M. Ruohoniemi, and R. A. Greenwald (1992), Substorm intensifications and field line resonances in the nightside magnetosphere, *J. Geophys. Res.*, *97*, 8495–8518, doi:10.1029/91JA03156.

Samson, J. C., L. L. Cogger, and Q. Pao (1996), Observations of field line resonances, auroral arcs, and auroral vortex structures, *J. Geophys. Res.*, *101*, 17,373–17,383, doi:10.1029/96JA01086.

Samsonov, A. A., D. G. Sibeck, B. M. Walsh, and N. V. Zolotova (2014), Sudden impulse observations in the dayside magnetosphere by THEMIS, *J. Geophys. Res. Space Physics*, *119*, 9476–9496, doi:10.1002/2014JA020012.

Sarris, T. E., et al. (2009), Characterization of ULF pulsations by THEMIS, *Geophys. Res. Lett.*, *36*, L04104, doi:10.1029/2008GL036732.

Sarris, T. E., W. Liu, X. Li, K. Kabin, E. R. Talaat, R. Rankin, V. Angelopoulos, J. Bonnell, and K. H. Glassmeier (2010), THEMIS observations of the spatial extent and pressure-pulse excitation of field line resonances, *Geophys. Res. Lett.*, *37*, L15104, doi:10.1029/2010GL044125.

Sarris, T. E., X. Li, W. Liu, E. Argyriadis, A. Boudouridis, and R. Ergun (2013), Mode number calculations of ULF field-line resonances using ground magnetometers and THEMIS measurements, *J. Geophys. Res. Space Physics*, *118*, 6986–6997, doi:10.1002/2012JA018307.

Shi, Q. Q., et al. (2013), THEMIS observations of ULF wave excitation in the nightside plasma sheet during sudden impulse events, *J. Geophys. Res. Space Physics*, *118*, 284–298, doi:10.1029/2012JA017984.

Shi, Q. Q., et al. (2014), Solar wind pressure pulse-driven magnetospheric vortices and their global consequences, *J. Geophys. Res. Space Physics*, *119*, 4274–4280, doi:10.1002/2013JA019551.

Shue, J., et al. (1998), Magnetopause location under extreme solar wind conditions, *J. Geophys. Res.*, *103*, 17,691–17,700, doi:10.1029/98JA01103.

Southwood, D., J. Dungey, and R. Etherington (1969), Bounce resonant interaction between pulsations and trapped particles, *Planet. Space Sci.*, *17*, 349–361, doi:10.1016/0032-0633(69)90068-3.

Southwood, D. J., and M. G. Kivelson (1981), Charged particle behavior in low-frequency geomagnetic pulsations 1. Transverse waves, *J. Geophys. Res.*, *86*, 5643–5655, doi:10.1029/JA086iA07p05643.

Sugiura, M., and C. Wilson (1964), Oscillation of the geomagnetic field lines and associated magnetic perturbations at conjugate points, *J. Geophys. Res.*, *69*(7), 1211–1216.

Takahashi, K., R. W. McEntire, A. Lui, and T. Potemra (1990), Ion flux oscillations associated with a radially polarized transverse Pc 5 magnetic pulsation, *J. Geophys. Res.*, *95*(A4), 3717–3731, doi:10.1029/JA095iA04p03717.

Takahashi, K., et al. (2010), Multipoint observation of fast mode waves trapped in the dayside plasmasphere, *J. Geophys. Res.*, *115*, A12247, doi:10.1029/2010JA015956.

Tan, L. C. (2004), Observation of magnetospheric relativistic electrons accelerated by Pc-5 ULF waves, *Geophys. Res. Lett.*, *31*, L14802, doi:10.1029/2004GL019459.

Tian, A. M., et al. (2012), Dynamics of long-period ULF waves in the plasma sheet: Coordinated space and ground observations, *J. Geophys. Res.*, *117*, A03211, doi:10.1029/2011JA016551.

Turner, D. L., Y. Shprits, M. Hartinger, and V. Angelopoulos (2012), Explaining sudden losses of outer radiation belt electrons during geomagnetic storms, *Nat. Phys.*, *8*, 208–212, doi:10.1038/nphys2185.

Wilken, B., C. K. Goertz, D. N. Baker, P. R. Higbie, and T. A. Fritz (1982), The SSC on July 29, 1977 and its propagation within the magneto-sphere, *J. Geophys. Res.*, *87*, 5901–5910, doi:10.1029/JA087iA08p05901.

Zhang, X. Y., Q. Zong, Y. F. Wang, H. Zhang, L. Xie, S. Y. Fu, C. J. Yuan, C. Yue, B. Yang, and Z. Y. Pu (2010), ULF waves excited by negative/positive solar wind dynamic pressure impulses at geosynchronous orbit, *J. Geophys. Res.*, *115*, A10221, doi:10.1029/2009JA015016.

Zong, Q., X. Zhou, X. Li, P. Song, S. Y. Fu, D. N. Baker, Z. Y. Pu, T. A. Fritz, P. Daly, A. Balogh, and H. Réme (2007), Ultralow frequency modulation of energetic particles in the dayside magnetosphere, *Geophys. Res. Lett.*, *34*, L12105, doi:10.1029/2007GL029915.

Zong, Q., X. Zhou, Y. F. Wang, X. Li, P. Song, D. N. Baker, T. A. Fritz, P. W. Daly, M. Dunlop, and A. Pedersen (2009), Energetic electron response to ULF waves induced by interplanetary shocks in the outer radiation belt, *J. Geophys. Res.*, *114*, A10204, doi:10.1029/2009JA014393.